Design and Application of a Data Driven controller using the Small-gain constraint for Positioning Control of a Nano-Positioner

T. D. Gupta, H. Habibullah, H. R. Pota and I. R. Petersen

Abstract— **In this paper, the design of a data driven controller using a small-gain theorem approach for improving the positioning accuracy of a piezoelectric tube scanner (PTS) is demonstrated. Open-loop frequency responses of both the X-PTS and Y-PTS are measured using a band-limited sweep sine signal and are used as primary data for this control design. The frequency response of the controllers is synthesized by the application of the small-gain theorem constraints over the entire frequency range for both the axes. The experimental implementation of this feedback data driven controller provides significant vibration reduction, with 19 dB and 15 dB damping at the resonance frequencies of the X and Y-axes of the PTS, respectively. A comparison between the open-loop and closed-loop tracking performance for triangular signals shows significant improvement up to the scanning frequency of 150 Hz. Moreover, the design of this data driven controller is less complex than conventional controller design methods as it does not need a system model.**

I. INTRODUCTION

The atomic force microscope (AFM) is a type of scanning probe microscope (SPM) which is capable of capturing high resolution images in different mediums, including vacuum, liquid and air [1], [2]. Over the last few decades, the AFM has had applications in many disciplines, such biological sciences, surface science and medical research. The capability of performing precision imaging at an atomic resolution, makes the AFM a suitable tool in nano-science applications [3], [4]. The basic components of an AFM comprise of an AFM head, cantilever (a sharp probe) and a piezo electric tube actuator. A sample is moved under a fixed cantilever to scan atomic resolution images of both electrically conductive and non-conductive samples. A laser beam emitted from a laser diode is reflected from the back of the cantilever tip and it is detected by a photodiode [5]. The amount of angular variation measured by the photodetector indicates the variation of the height of the sample surface. The movement of the PTS along the Z-axis is governed by the output of the photodiode and the movement of the PTS along the X and Y-axes depends on the voltages applied to the respective directions [1]. The precision tracking of the reference signals along the X and Y-axes is limited due to vibration effects, creep, hysteresis effects and cross coupling effects [6], [7]. The nonlinear hysteresis effect that occours due to the application of high voltages to the X and Y-axes, can be around 10-15 percent of the total displacement in a long traversal motion [8]. The cross-coupling effect in the PTS occurs due to its collocated structure, which distorts the scanned image [9]. Additionally, during slow scanning the creep effect becomes dominant, which adversely affects the vertical positioning of the sample [10].

In the traditional raster scanning method, a triangular signal is applied along the X-axis with a slowly increasing staircase or ramp signal along the Y-axis. The main problem with the raster scanning method is that the triangular signal contains all the odd harmonics of the fundamental frequency. Then the imaging performance of an AFM is limited by the vibration of the PTS, due to the excitation of its lightly damped resonant modes by the higher harmonics of the triangular reference signal [11]. The low resonant frequency of PTS limits the system bandwidth and scanning speed of an AFM. The scanning speed for most commercially available AFMs is limited to 1 percent of the first resonance frequency of the PTS [12].

In commercially available AFMs, a proportional integral (PI) controller is used for nanopositioning control. Generally, the performance of the PI controller is reasonably good for low frequency applications, as the closed-loop bandwidth is limited. The maximum closed-loop bandwidth that can be typically achieved by using a PI controller is less than $2\zeta w_n$, where ζ is the damping constant of PI controller and w_n is the first resonance frequency of the PTS. The normal value of the damping constant for a PI controller is 0.01 and the first resonance frequency of PTS is usually around 1 kHz, which means the scanning speed is limited to 10 Hz [13].

Many approaches have been undertaken by researchers to mitigate the effect of vibration in the PTS. Some of those approaches have damped the resonant peak significantly, but still suffer from the problems of limited bandwidth and poor tracking of the reference signal. It is essential to overcome this problem to increase imaging quality and the AFM's scanning speed. A signal transformation method is used to track the reference triangular signal in [14]. As this method does not damp the resonant peak by a significant amount, its performance is limited to low frequencies. An integral resonant controller (IRC) can provide a scanning speed of $0.1 f_r$, while suppressing the resonant mode of the PTS, where f_r is the first resonant frequency of PTS [15]. An LQG controller shows improved positioning performance upto 125 Hz by reducing the first resonant peak, while giving better tracking results than a PI controller [12].

The data driven controller approach is a recent approach,

*This work was supported by the Australian Research Council under grant DP160101121.

T. D. Gupta, H. Habibullah and H. R. Pota are with the School of EIT, University of New South Wales, Canberra, ACT, 2612, Australia. Tanmoy.DasGupta@student.adfa.edu.au, habibruet05@gmail.com, h.pota@adfa.edu.au

I. R. Petersen is with the Research School of Engineering, Australian National University. i.r.petersen@gmail.com

where prior identification of the plant transfer function is not necessary [16], [17]. A reference tracking data driven controller is designed based on a H_2 approach in [18]. In this control design method, measured input/output data is only required to guarantee the specific system performance. A data driven controller can be synthesized without constructing a transfer function or state-space model of the plant. Model identification is a major challenge in traditional controller design methods [19], [20]. The stability, robustness and convergence of the closed-loop system can be guaranteed by mathematical analysis of the input/output data of the controlled system under specified constraints [21], [22], [23]. Data driven controller design reduces the complexity of the controller design problems. The main problem associated with data driven controller design is ensuring the closed-loop system stability for the designed controller.

In the proposed design process, frequency response data of the SISO system for the AFM is measured by using a band-limited swept sine signal. The controller frequency response is calculated by minimizing the error between the reference input and observed position output of the closed-loop system at each frequency, which leads to the damping of the first resonant peak.

The design process imposes small-gain constraints on the controller frequency response. The small-gain theorem states that if the loop gain corresponding to two stable systems is strictly less than one, then their feedback interconnection will be stable [24], [25]. From the frequency responses of both the X-PTS and Y-PTS it is observed that, PTSs have very high gains for a small range of frequencies near the resonant frequencies. The highest resonant peak is mainly responsible for creating vibrations in the PTS. Small-gain constraints force the controller gain in the resonant region to be low. The amount of damping obtained is higher for much a lower gain within this frequency range.

In this work, a data driven controller based on the small-gain theorem is proposed to reduce the vibration effect of the PTS. The open-loop frequency response data for the position sensors in both the X and Y-directions is used in calculating the controller frequency response. An optimization problem is formulated based on the reference input and error. In addition, the small-gain constraints ensure closed-loop stability of the PTS system. Finally, by using the Prediction Error Minimization (PEM) approach, the controller transfer function was identified. Practical implementation of the proposed controller on an AFM shows a significant amount of damping of the first resonant peak, as well as a good tracking of the reference input for different scanning frequencies (upto 150Hz) for both the X and Y-axes tracking.

The remainder of the paper is organized as follows: The experimental setup and data acquisition method is presented in Section II, the controller design procedure is discussed in Section III, and Section IV presents the experimental results. Finally, Section V concludes the paper.

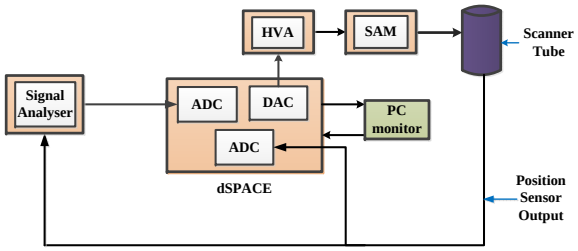

Fig. 1. Block diagram of the experimental setup used in AFM nano-positioning.

II. EXPERIMENTAL SETUP AND DATA ACQUISITION

The experimental setup for the proposed scheme consists of: 1) an NT-MDT Ntegra scanning probe microscope (SPM) in which the PTS is placed; 2) a dual channel dynamic signal analyzer (SA) HP35665A to measure the frequency response between the reference input and the X and Y axes capacitive position sensor outputs; 3) a DSPACE system for the digital implementation of the controller with a sampling frequency of 80 kHz; 4) a high-voltage amplifier (HVA) with a constant gain of 15 which supplies power to the PTS ; 5) a signal access module which allows direct connection to the PTS electrodes; 5) a vibration isolator TS150 to isolate the AFM from the effect of external vibrations; 6) control electronics; 7) a computer to operate the AFM's NOVA in-built software. A scan-by-sample scanner z13037cl is used, which performs the scanning in constant force contact mode. The usual scanning range is 100 μm $\times$ 100 μm $\times$ 10 μm and the resonant frequency for X and Y axes is approximately 800-910Hz and 5 kHz in the Z-direction. The displacements in the X, Y, Z directions are sensed by capacitive sensors. The experimental setup shown in Fig. 1 gives the interconnection between all components.

In the proposed design scheme, input-output logarithmic frequency responses of both the X-axis and Y-axis PTS have been generated using the SA and processed in MATLAB. The measured frequency responses of the X-PTS and Y-PTS are shown in Fig. 2(a) and Fig. 2(b), respectively. The resonant peak for the X-PTS is at 813 Hz and the two resonant peaks of the Y-PTS are at 780 Hz and 903 Hz. To avoid vibration effects, the open-loop scanning speed is limited to around 8-9 Hz which is around 100 times less than the resonant frequencies. For the data driven controller design, the measured frequency response of the PTS is used to determine the frequency response of the required controller.

III. CONTROLLER DESIGN

This section provides a brief description of the data driven controller design using the small-gain constraints. In order to guarantee robustness and stability of the closed-loop PTS system, a positive feedback interconnection is considered to design the controller as shown in Fig. 3. From the block diagram in Fig. 3, the relationship between the reference

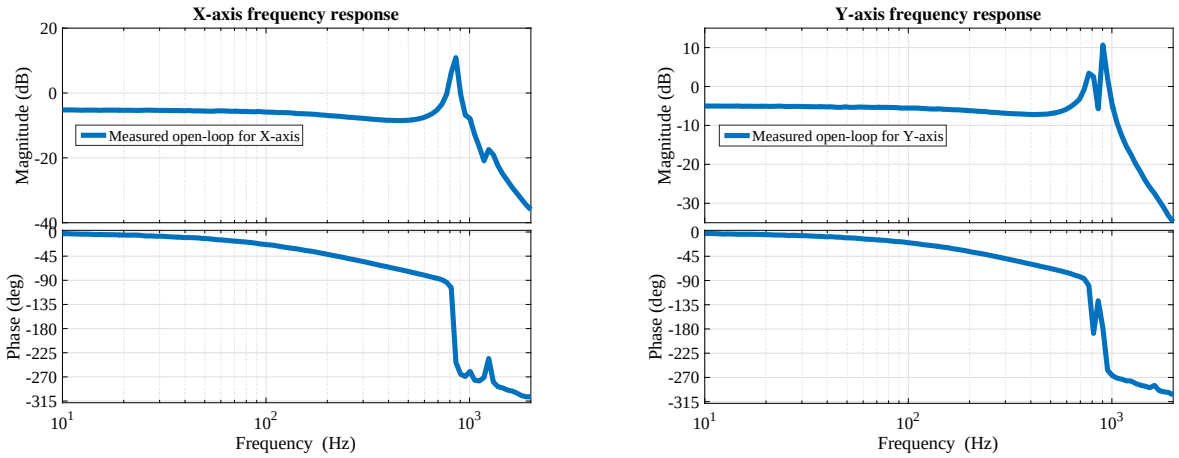

(a) (b)

Fig. 2. Measured frequency response plot (a) input to the X-PTS and output from the X position sensor (b) input to the Y-PTS and output from the Y position sensor.

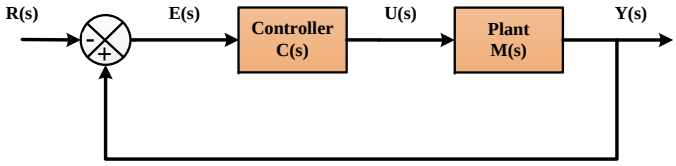

Fig. 3. Closed-loop system with the data-driven controller.

input, system output and the error can be calculated as follows:

$$Y(s) = \frac{-M(s)C(s)}{1-M(s)C(s)}R(s); \tag{1}$$

$$E(s) = \frac{-1}{1-C(s)M(s)}R(s). \tag{2}$$

Here $Y(s)$ is the measured output signal, $C(s)$ is the controller transfer function, $E(s)$ is the error signal and $M(s)$ is transfer function of the PTS. To get good tracking performance, our main objective is to reduce the error function given in (2). From the block diagram shown in Fig. 3 we obtain the following transfer function matrix (where U(s) is the control input):

$$\begin{bmatrix} E(s) \\ Y(s) \end{bmatrix} = \begin{bmatrix} M_{11}(s) & M_{12}(s) \\ M_{21}(s) & M_{22}(s) \end{bmatrix} \begin{bmatrix} R(s) \\ U(s) \end{bmatrix}; \tag{3}$$

$$\begin{aligned} E(s) &= M_{11}(s)R(s) + M_{12}(s)U(s) \\ &= -R(s) + M(s)U(s); \\ Y(s) &= M_{21}(s)R(s) + M_{22}(s)U(s) \\ &= M(s)U(s); \\ U(s) &= C(s)E(s). \end{aligned} \tag{4}$$

Using (4), the relationship between $R(s)$ and $E(s)$ is given as follows:

$$E(s) = (-1 + M(s)N(s))R(s) \tag{5}$$

where $N(s) = C(s)(C(s)M(s)-1)^{-1}$.
The control objective is to choose the frequency response $C(j\omega)$ at each frequency by minimizing the norm of the transfer function matrix from $R(s)$ to $E(s)$. Two constraints have been applied over the entire frequency region. For both the X-axis PTS and Y-axis PTS, the same design procedure is followed. The controller design procedure is discussed in detail in the following section:

A. Controller design using the small-gain theorem

The minimization of the error function subject to small-gain constraints gives the optimum value for the controller magnitude and phase for each frequency between 10 Hz and 2000 Hz. The main motivation for applying the small-gain theorem for the entire frequency region is to ensure stability of the closed-loop system. The optimization problem is described as follows:

$$\min_{C(j\omega)} \| -1 + M(j\omega)N(j\omega)\|^2 \tag{6}$$

subject to

$$\|C(j\omega)\|^2 \|M(j\omega)\|^2 < 1, \tag{7}$$

$$\|C(j\omega)\|^2 \leq \mu. \tag{8}$$

The first constraint (7) is SG constraint that ensures that the loop gain of the system remains less than unity for the calculated controller. The second constraint (8) limits the gain of the controller. Normally, zero steady state error is achieved by designing infinite gain controller. This is not practical as it creates complexity in system realizability. By limiting the gain of the controller to a certain value

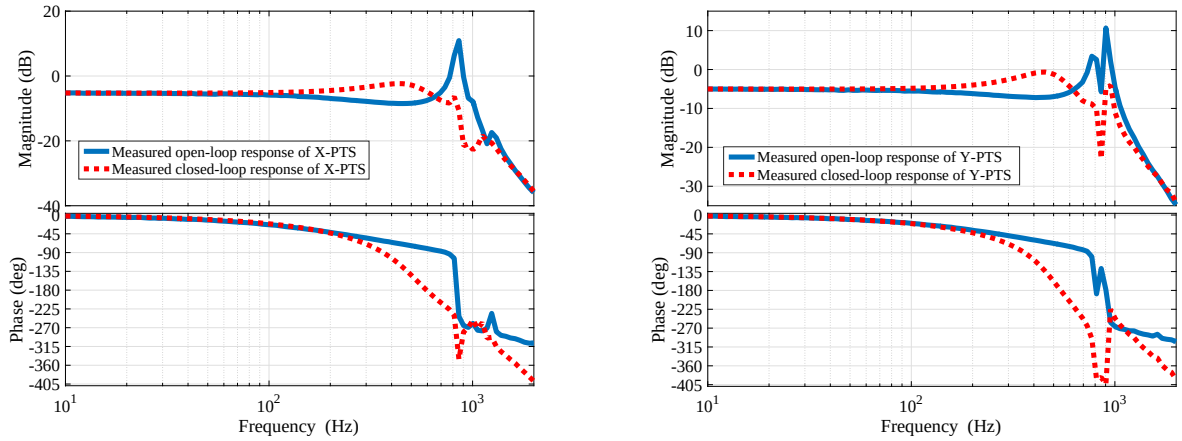

(a) (b)

Fig. 4. A comparison of the vibration damping between the open-loop and closed-loop (a) input to the X-PTS and output from the X position sensor (b) input to the Y-PTS and output from the Y position sensor.

ensures easier system realization. The non-convexity of this optimization problem has been addressed by replacing $C(j\omega)$ by $N(j\omega)$ as follows:

$$\begin{aligned} N(j\omega) &= C(j\omega)(C(j\omega)M(j\omega)-1)^{-1}; \\ C(j\omega) &= N(j\omega)(M(j\omega)N(j\omega)-1)^{-1}. \end{aligned} \tag{9}$$

Then the constraint from (7) changes to:

$$\begin{aligned} &\|C(j\omega)\|^2\|M(j\omega)\|^2 < 1; \\ &\Leftrightarrow C(j\omega)C^*(j\omega)M(j\omega)M^*(j\omega) < 1; \\ &\Leftrightarrow (N^*(j\omega)M^*(j\omega)-1)^{-1}N^*(j\omega)N(j\omega) \\ &\qquad \times (M(j\omega)N(j\omega)-1)^{-1}M(j\omega)M^*(j\omega) < 1; \\ &\Leftrightarrow M^*(j\omega)N^*(j\omega)+M(j\omega)N(j\omega) < 1; \end{aligned} \tag{10}$$

It is assumed that, $M(j\omega) = A + jB$, $N(j\omega) = a + jb$. Then the non-linear inequality (10) simplifies to:

$$2aA - 2bB < 1. \tag{11}$$

Similarly, the second constraint (8) can be rewritten in a convex form as follows:

$$\begin{aligned} &\|C(j\omega)\|^2 \le \mu; \\ &\Leftrightarrow C(j\omega)C^*(j\omega) \le \mu; \\ &\Leftrightarrow (N^*(j\omega)M^*(j\omega)-1)^{-1}N^*(j\omega)N(j\omega) \\ &\qquad \times (M(j\omega)N(j\omega)-1)^{-1} \le \mu; \\ &\Leftrightarrow N^*(j\omega)(1-\mu M(j\omega)M^*(j\omega))N(j\omega) \\ &\qquad +\mu(M^*(j\omega)N^*(j\omega)+M(j\omega)N(j\omega)) \le \mu; \\ &\Leftrightarrow (a^2+b^2)(1-\mu(A^2+B^2))+2\mu(aA-bB) \le \mu. \end{aligned} \tag{12}$$

In solving the aforementioned optimization problem, the MATLAB built-in function *fmincon* was applied. The main motivation behind choosing *fmincon* for minimizing (6) is that it can minimize a non-linear function subject to inequality constraints. The Interior-Point algorithm is chosen among the four available algorithms (Interior-Point, Trust-Region-Reflective, SQP, SQP-legacy, Active-Set) in fmincon, which gives better results for convergence [26]. In the solution of the optimization problem, the selection of the parameter μ is critical. As the value of μ increases, the better is the closed-loop response, reducing the error between the reference input and the output. However, for higher values of μ the controller identification becomes more difficult. For feasible implementation of the controller, a suitable value of μ is selected, which can provide good tracking performance while giving an easily identifiable frequency response for the controller. At each frequency point of the open-loop response, the optimization is done to find $N(j\omega)$. Hence, the controller frequency response data $C(j\omega)$ can be calculated from (9).

B. Identification of the Controller Response

The MATLAB System Identification Toolbox is used to identify the transfer function for the proposed controllers for both the X-PTS and Y-PTS. The controller is identified using a frequency domain Prediction Error Minimization (PEM) estimation method. The controller transfer function for the X-PTS is identified as follows:

$$C_x(s) = \frac{1.734e04s^2 - 6.935e06s + 5.999e11}{s^3 + 1.706e04s^2 + 1.052e08s + 3.46e11}.$$

Similarly, the same procedure is applied to design the controller for the Y-PTS. The transfer function for the Y-PTS control is identified as follows:

$$C_y(s) = \frac{-1.72s^4 + 3301s^3 - 1.252e08s^2 + 1.248e11s - 2.237e15}{s^4 + 1.684e04s^3 + 1.402e08s^2 + 5.947e11s + 1.275e15}.$$

IV. EXPERIMENTAL RESULTS

A. Damping Performance

The proposed data driven controller is implemented on an AFM and its performance has been evaluated by measuring

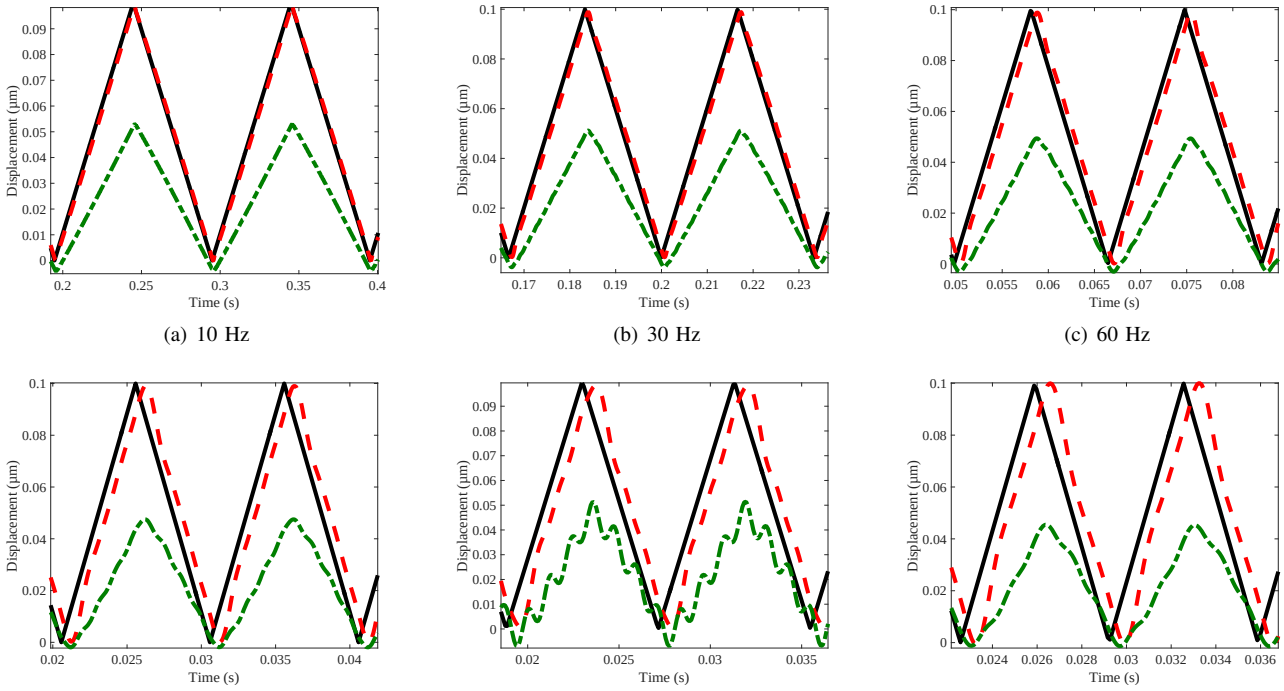

(a) 10 Hz (b) 30 Hz (c) 60 Hz

(d) 100 Hz (e) 120 Hz (f) 150 Hz

Fig. 5. Reference input (black solid line), open-loop (green dashed-dotted line) and closed-loop (dashed red line) X sensor output at different frequencies in the implementation of the proposed controller.

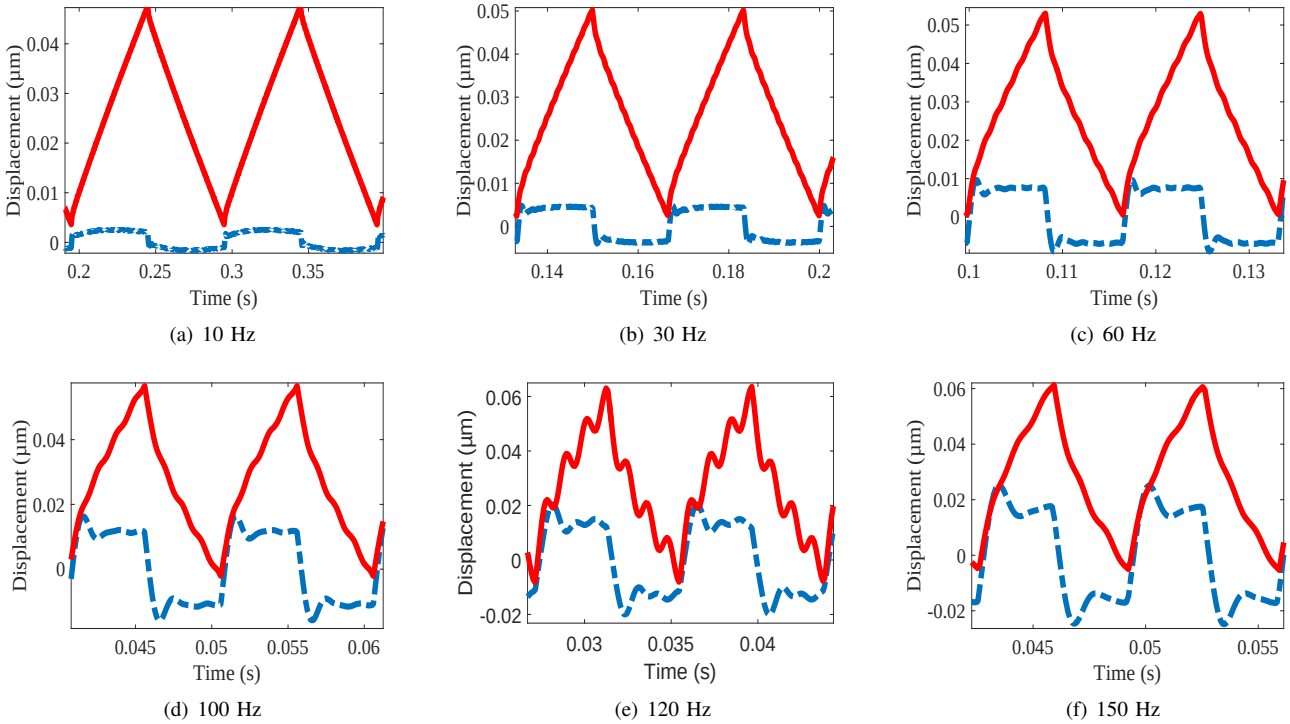

(a) 10 Hz (b) 30 Hz (c) 60 Hz

(d) 100 Hz (e) 120 Hz (f) 150 Hz

Fig. 6. Open-loop error (red solid line) and closed-loop error (dashed-dotted blue line) between the reference input and X sensor output at different frequencies in the implementation of the proposed controller.

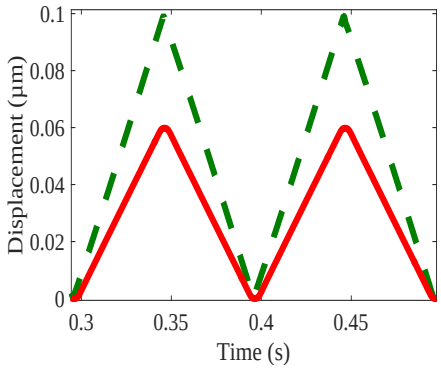

(a) 10 Hz

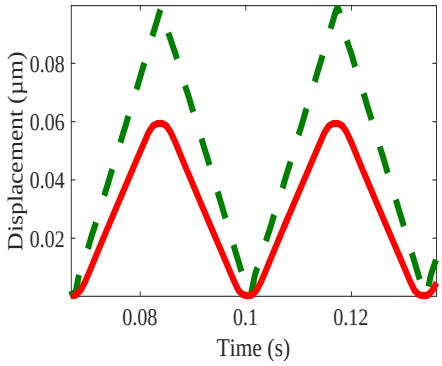

(b) 30 Hz

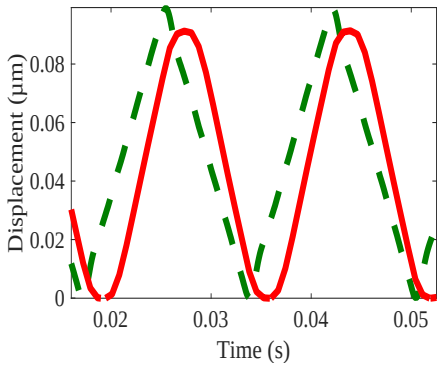

(c) 60 Hz

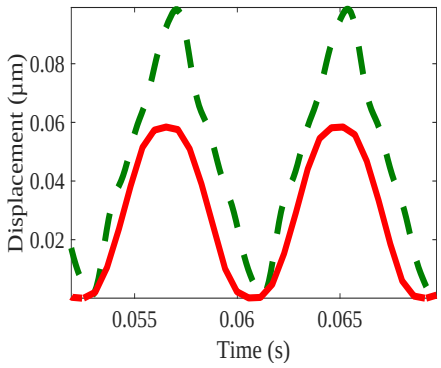

(d) 120 Hz

Fig. 7. Comparison of X-axis tracking performance between the proposed controller (green solid line) and the built-in PI controller (red dotted line) at different frequencies.

the open-loop and closed-loop frequency responses on the both X and Y-axes. The controller provides significant damping at the resonant peaks, while reducing the vibration effects in the PTS along the lateral axes. The open-loop and closed-loop responses are shown in Fig. 4(a) for the X-PTS and in Fig. 4(b) for the Y-PTS. The first resonant peak is damped by 19 dB in the X-PTS by using the proposed controller. This result can be observed from Fig. 4(a). Similarly in the Y-PTS, 15 dB damping of the first resonant peak and 12 dB damping of second resonant peaks are achieved, as can be seen in Fig. 4(b).

B. Tracking Performance

To illustrate the proposed controller's performance in the time domain, a set of triangular signals with different frequencies (10, 30, 60, 100, 120 and 150 Hz) are generated using the dSPACE system and applied along the X-direction of the PTS. The reference input, open-loop and closed-loop output are shown in each of the figures from Fig. 5(a)-(f). The result in Fig. 5 shows excellent tracking of the reference input compared to the open-loop response. Moreover, the oscillatory motion of the open-loop response is reduced by a significant amount as shown in Fig. 5(e). Furthermore, the comparisons between open-loop error and closed-loop error are shown in Fig. 6(a)-(f). The error signal is found from difference between the reference input and output of the position sensor. Fig. 6 shows that, the magnitudes of the closed-loop errors are small compared to the magnitudes of the open-loop errors. The closed-loop tracking of triangular signal by the proposed controller and the built-in PI controller at different frequencies (10 Hz, 30 Hz, 60 Hz and 120 Hz) are shown in Fig.7. From Fig.7, it can be seen that the PI controller response is being deviated from triangular shape to sinusoidal shape as the frequency is increased. Therefore, the proposed scheme shows better tracking performance compared to the existing PI controller of the AFM.

V. CONCLUSION

In this paper, a data-driven controller is designed and implemented on an AFM. By the application of small-gain contraints and input-output error minimization, the proposed controller is designed to reduce vibration effects in the PTS. This SISO based data-driven controller provides significant damping performance for both the X-PTS (19 dB damping of the first resonant peak) and Y-PTS (15 dB damping of the first resonant peak and 12 dB damping of the second resonant peak). The controller shows an excellent closed-loop tracking of triangular signals upto 150 Hz along the X-direction of the PTS. In future, this controller will be extented to multi-input multi-output (MIMO) systems for high speed imaging performance and reduction of cross-coupling effects.

REFERENCES

[1] S. Salapaka, A. Sebastian, J. P. Cleveland, and M. V. Salapaka, "High bandwidth nano-positioner: A robust control approach," *Review of scientific instruments*, vol. 73, no. 9, pp. 3232–3241, 2002.

[2] G. Binnig and D. P. Smith, "Single-tube three-dimensional scanner for scanning tunneling microscopy," *Review of Scientific Instruments*, vol. 57, no. 8, pp. 1688–1689, 1986.

[3] B. Kim, G. Pyrgiotakis, J. Sauers, and W. M. Sigmund, "The effect of monolayers alkyl chain length on atomic force microscopy anodization lithography," *Colloids and Surfaces A: Physicochemical and Engineering Aspects*, vol. 253, no. 10–3, pp. 23–26, Dec. 2005.

[4] H. Habibullah, H. R. Pota, and I. R. Petersen, "High-precision spiral positioning control of a piezoelectric tube scanner used in an atomic force microscope," in *American Control Conference (ACC), 2014*, 2014, pp. 1625–1630.

[5] G. Binnig, C. F. Quate, and C. Gerber, "Atomic force microscope," *Phys. Rev. Lett.*, vol. 56, issue 9, pp. 930–933, Mar. 1986.

[6] M. Ratnam, B. Bhikkaji, A. Fleming, and S. Moheimani, "PPF control of a piezoelectric tube scanner," in *Proceedings of the 44th IEEE Conference on Decision and Control*. IEEE, 2005, pp. 1168–1173.

[7] S. K. Das, H. R. Pota, and I. R. Petersen, "Resonant controller for fast atomic force microscopy," in *2012 IEEE 51st IEEE Conference on Decision and Control (CDC)*. IEEE, 2012, pp. 2471–2476.

[8] H. Habibullah, H. R. Pota, and I. R. Petersen, "High-speed spiral imaging technique for an atomic force microscope using a linear quadratic gaussian controller," *Review of Scientific Instruments*, vol. 85, no. 3, p. 033706, 2014.

[9] H. Habibullah, H. R. Pota, I. R. Petersen, and M. S. Rana, "Creep, hysteresis, and cross-coupling reduction in the high-precision positioning of the piezoelectric scanner stage of an atomic force microscope," *IEEE Transactions on Nanotechnology*, vol. 12, no. 6, pp. 1125–1134, 2013.

[10] H. Habibullah, H. R. Pota, and I. R. Petersen, "LQG controller with a vibration compensator for the lateral positioning of an AFM scanner," in *2012 2nd Australian Control Conference (AUCC)*, 2012, pp. 324–329.

[11] S. K. Das, H. R. Pota, and I. R. Petersen, "Multi-variable resonant controller for fast atomic force microscopy," in *Control Conference (AUCC), 2012 2nd Australian*. IEEE, 2012, pp. 448–453.

[12] H. Habibullah, H. Pota, I. R. Petersen, and M. Rana, "Tracking of triangular reference signals using lqg controllers for lateral positioning of an afm scanner stage," *IEEE/ASME Transactions on Mechatronics*, vol. 19, no. 4, pp. 1105–1114, 2014.

[13] B. Bhikkaji, S. Moheimani *et al.*, "Fast scanning using piezoelectric tube nanopositioners: a negative imaginary approach— nova. the university of newcastle's digital repository," 2009.

[14] A. Bazaei, Y. K. Yong, S. R. Moheimani, and A. Sebastian, "Tracking of triangular references using signal transformation for control of a novel afm scanner stage," *IEEE Transactions on Control Systems Technology*, vol. 20, no. 2, pp. 453–464, 2012.

[15] B. Bhikkaji and S. R. Moheimani, "Integral resonant control of a piezoelectric tube actuator for fast nanoscale positioning," *IEEE/ASME Transactions on mechatronics*, vol. 13, no. 5, pp. 530–537, 2008.

[16] J. J. M. van Helvoort, "Unfalsified control: Data-driven control design for performance improvement," *Technische Universiteit Eindhoven, Eindhoven, Netherlands*, 2007.

[17] M.-B. Radac and R.-E. Precup, "Model-free constrained data-driven iterative reference input tuning algorithm with experimental validation," *International Journal of General Systems*, vol. 45, no. 4, pp. 455–476, 2016.

[18] A. S. Bazanella, L. Campestrini, and D. Eckhard, *Data-driven controller design: the H2 approach*. Springer Science & Business Media, 2011.

[19] L. Campestrini, D. Eckhard, A. S. Bazanella, and M. Gevers, "Data-driven model reference control design by prediction error identification," *Journal of the Franklin Institute*, 2016.

[20] Y.-g. Li, J. Shen, K. Lee, X.-c. Liu, and W.-z. Fei, "Data-driven nonlinear control of a solid oxide fuel cell system," *Journal of Central South University*, vol. 19, no. 7, pp. 1892–1901, 2012.

[21] Z.-S. Hou and Z. Wang, "From model-based control to data-driven control: Survey, classification and perspective," *Information Sciences*, vol. 235, pp. 3–35, 2013.

[22] Z. Hou and S. Jin, "Data-driven model-free adaptive control for a class of mimo nonlinear discrete-time systems," *IEEE Transactions on Neural Networks*, vol. 22, no. 12, pp. 2173–2188, 2011.

[23] D. Eckhard and A. S. Bazanella, "Robust convergence of the steepest descent method for data-based control," *International Journal of Systems Science*, vol. 43, no. 10, pp. 1969–1975, 2012.

[24] C. A. Desoer and M. Vidyasagar, *Feedback systems: input-output properties*. Siam, 2009, vol. 55.

[25] M. Green and D. J. Limebeer, *Linear robust control*. Courier Corporation, 2012.

[26] N. Brixius, F. A. Potra, and R. Sheng, "Sdpha: A matlab implementation of homogeneous interior-point algorithms for semidefinite programming," *Optimization Methods and Software*, vol. 11, no. 1-4, pp. 583–596, 1999.